

Intermolecular Interactions in π -Stacked Conjugated Molecules. Synthesis, Structure, and Spectral Characterization of Alkyl Bithiazole Oligomers

Amy B. Koren, M. David Curtis,* Anthony H. Francis, and Jeff W. Kampf

Contribution from the Department of Chemistry, University of Michigan,
Ann Arbor, Michigan 48109-1055

Received November 4, 2002; E-mail: mdc Curtis@umich.edu

Abstract: Syntheses are reported of new 4,4'-dialkyl-2,2'-bithiazole oligomers that have alkenoxy side chains that are capable of easy conversion to oligomers with functionalized side chains, e.g., terminally substituted hydroxy chains. The crystal structures of two representative oligomers (4,4',4'',4'''-tetra-(2-propenoxymethyl)-2,2',5',5'',2'',2'''-quaterthiazole (**3P2**) and 4,4',4'',4'''-tetra-(3-hydroxypropyloxymethyl)-2,2',5',5'',2'',2'''-quaterthiazole (**3H2**)) were determined; **3P2** crystallizes in a π -stacked motif with two molecules per unit cell, whereas **3H2** forms π -stacks that are linked with hydrogen bonds to form infinite two-dimensional sheets with one molecule per unit cell. A comparison of the UV-vis spectra of the compounds in solution and in the solid state provides unequivocal evidence for the presence of a Davydov splitting, $W_D \approx 0.2$ eV, in solid **3P2**. The spectra are interpreted in the framework of molecular exciton theory to extract a value of the intermolecular transfer integral, $J \approx 0.2$ eV, for a total exciton bandwidth of ca. 0.8 eV. Monte Carlo calculations were used to determine the density of states of the exciton band and the absorption and emission line shapes of the 0-0 transition. It is suggested that the "three-humped" absorption profile typical of partially crystalline, regioregular polymers is the "optical signature" of π -stacking.

Introduction

There are currently intensive research efforts devoted to the basic science and development of organic conjugated molecules as the active materials for thin-film transistors (OTFTs),¹ light-emitting diodes (OLEDs),² and photovoltaic diodes (OPVDs).^{3,4} The unique properties of organic materials—e.g., their solution processibility, especially spin coating and ink-jet or screen printing techniques, ease of alteration of properties, etc.—make them more attractive than inorganic semiconductors for applications that require large area coverage, structural flexibility, or low-cost, reel-to-reel manufacture. Outstanding progress has been made in fabricating OTFTs with mobilities as high as $1.5 \text{ cm}^2 \text{ V}^{-1} \text{ s}^{-1}$ for thin-film pentacene devices at room temperature.⁵ This mobility is comparable to that of amorphous silicon. Such large values imply the existence of coherent bandlike transport and a reasonably wide conduction band.⁶ The hole bandwidth has been estimated from experimental data and from

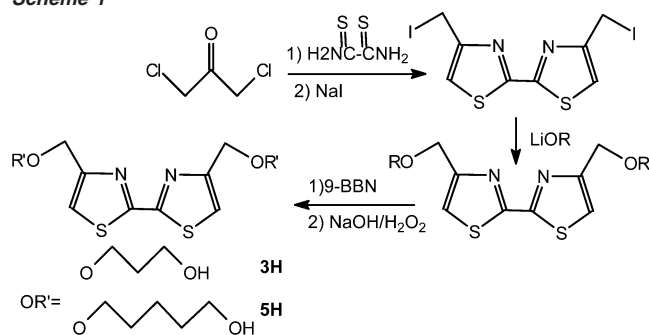
INDO calculations to be $\sim 500 \text{ meV}$.⁷ At higher temperatures, coupling to phonons causes a decrease in the bandwidth W , until $W \approx kT$ near room temperature, at which point the conductivity mechanism becomes activated hopping.⁸

The impressive performance of pentacene and related oligomers (tetracene, sexithiophene (T_6), etc.) notwithstanding, these molecules may not have the "ideal" solid-state morphology to produce maximum carrier mobility. The crystal structures of all these molecules share the so-called "herringbone" motif, in which the molecules are packed more or less edge-to-face in two-dimensional (2-D) layers.⁹ The highest mobilities are in the 2-D layers.¹⁰ However, the edge-to-face packing minimizes π - π overlap between adjacent molecules, thus decreasing the carrier bandwidth, which, for a one-dimensional (1-D) chain, is given by $W = 4J$, where J is the intermolecular π - π coupling constant and is defined as $J = \int \psi V_{\text{int}} \psi' d\tau$.^{6,11} Therefore, there exists the possibility that higher mobilities at room temperature

- (1) (a) Dimitrakopoulos, C. D.; Malenfant, P. R. L. *Adv. Mater.* **2002**, *14*, 99. (b) Horowitz, G. *Adv. Mater.* **1998**, *10*, 365. (c) Horowitz, G. *J. Mater. Chem.* **1999**, *9*, 2021. (d) Katz, H. E.; Bao, Z. *J. Phys. Chem. B* **2000**, *104*, 671. (e) Lovinger, A. J.; Rothberg, L. J. *J. Mater. Res.* **1996**, *11*, 1581.
- (2) (a) Hudson, A. J.; Weaver, M. S. In *Functional Organic and Polymeric Materials*; Richardson, T. H., Ed.; John Wiley & Sons: New York, 2000. (b) Mitschke, U.; Bäuerle, P. *J. Mater. Chem.* **2000**, *10*, 1471.
- (3) Kaneko, M. In *Handbook of Organic Conductive Molecules and Polymers*, Vol. 4; Nalwa, H. S., Ed.; Wiley: New York, 1997.
- (4) (a) Brabec, C. J.; Sariciftci, S. N. *Monatsh. Chem.* **2001**, *132* (4), 421. (b) Shirota, Y. *J. Mater. Chem.* **2000**, *10*, 1.
- (5) Lin, Y.-Y.; Gundlach, D. J.; Nelson, S.; Jackson, T. N. *IEEE Electron Device Lett.* **1997**, *18*, 606.
- (6) Kittel, C. *Introduction to Solid State Physics*, 7th Ed.; John Wiley & Sons: New York, 1996; Chapters 7–9.

- (7) (a) Cornil, J.; Beljonne, D.; Calbert, J.-P.; Brédas, J.-L. *Adv. Mater.* **2001**, *13*, 1053. (b) Brédas, J.-L.; Beljonne, D.; Cornil, J.; Calbert, J.-P.; Shuai, Z.; Silbey, R. *Synth. Met.* **2002**, *125*, 107.
- (8) (a) Holstein, T. *Ann. Phys.* **1959**, *8*, 325. (b) see ref 8a, 343.
- (9) (a) Campbell, R. B.; Trotter, J.; Robertson, J. M. *Acta Crystallogr.* **1961**, *14*, 705. (b) Horowitz, G.; Bachet, B.; Yassar, A.; Lang, P.; Demanze, F.; Fave, J. L.; Garnier, F. *Chem. Mater.* **1995**, *7*, 1337. (c) Siegrist, T.; Fleming, R. M.; Haddon, R. C.; Laudise, R. A.; Lovinger, A. J.; Katz, H. E.; Bridenbaugh, P.; Davis, D. D. *J. Mater. Res.* **1995**, *10*, 2170.
- (10) (a) Sirringhaus, H.; Brown, P. J.; Friend, R. H.; Nielsen, M. M.; Bechgaard, K.; Langeveld-Voss, B. M. W.; Spierling, A. J. H.; Jansen, R. A. J.; Meier, E. W.; Herwig, P.; de Leeuw, D. M. *Nature* **1999**, *401*, 685. (b) Österbacka, R.; An, C. P.; Jiang, X. M.; Vardeny, Z. V. *Science* **2000**, *287*, 839. (c) Lee, K.; Heeger, A. J. *Synth. Met.* **2002**, *128*, 279.
- (11) Pope, M.; Swenberg, C. E. *Electronic Processes in Organic Crystals and Polymers*, 2nd Ed.; Oxford University Press: New York, 1999.

Scheme 1



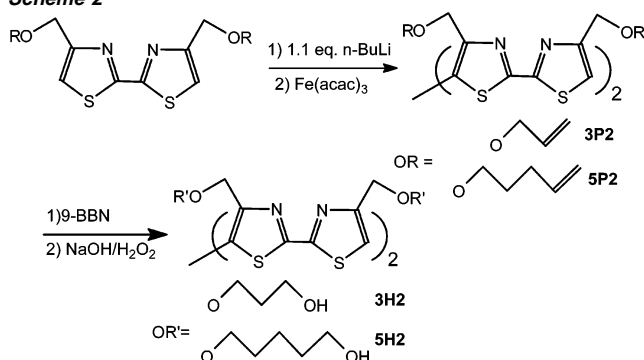
may be achieved by designing conjugated molecules that stack face-to-face (π -stack) in the solid state, thereby increasing the intermolecular interaction, $J > kT$.^{7,12} In addition to having a π -stacked morphology, the ideal OTFT material would self-assemble on the surface of a substrate (e.g., the gate dielectric of a field effect transistor (FET)) so that the π -stacks would be parallel to the surface, i.e., the direction of highest mobility would coincide with the direction of current flow in the FET.^{10a,13}

We and others have determined the solid-state structures of several oligomers and polymers based on 4,4'-dialkyl-2,2'-bithiazoles (ABTZs).^{14,15} These materials invariably exhibit a π -stacked morphology. In this paper, we report the synthesis, structure, and spectroscopic characterizations of some ABTZ oligomers that were designed to self-assemble with π -stacks parallel to a hydrophilic surface by means of hydrogen bonding between hydroxyl groups placed on the termini of the alkyl side chains and polar groups on the surface. (The characterization of the oriented films will be reported elsewhere.¹⁶) In particular, a comparison of the UV-vis spectra of the same oligomer chromophore in different crystalline environments provides unequivocal evidence for the influence of intermolecular (π - π) interactions on the spectra of conjugated molecules in the solid state.

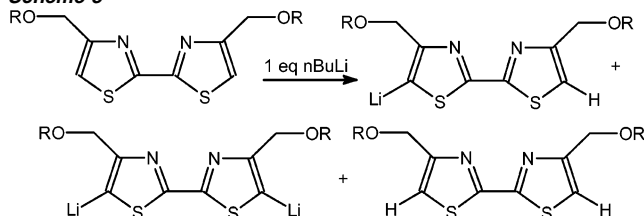
Results and Discussion

One goal of this research was the preparation of conjugated oligomers and polymers with polar groups located on the side chains. To expedite the syntheses, we chose to first synthesize a halomethyl-substituted bithiazole that could be used as a substrate onto which various side groups could be introduced. This procedure eliminated the necessity of preparing a new bithiazole for every desired side chain. The synthetic strategy is illustrated in Schemes 1 and 2. The synthesis of 4,4'-

Scheme 2



Scheme 3



chloromethyl-2,2'-bithiazole had an unusually low yield, which was ascribed to the fact that each chloromethyl group on the starting material, 1,3-dichloroacetone, can react with dithioamide to give a large number of oligomeric products. The desired product, 4,4'-dichloromethyl-2,2'-bithiazole, was easily separable from the resultant mixture, only because it sublimed and the other products did not. The chloro groups in the dichloromethylbithiazole proved to be resistant to nucleophilic substitution by lithium alkoxides in tetrahydrofuran (THF). Therefore, the bis(iodomethyl)bithiazole was synthesized through halogen exchange to make the methylene group more susceptible to substitution by alkoxides. From the bis(iodomethyl)bithiazole, the bithiazoles with alkenoxy side chains were prepared as shown in Schemes 1 and 2.

The dimerization reactions of the alkene-substituted monomers shown in Scheme 2 produced a mixture of monomer, dimer, and other higher-molecular-weight oligomers. The desired dimer was obtained in a yield of only $\sim 50\%$. Apparently, the lithiation of the bithiazole by 1 equiv of butyllithium produced a mixture of mono-, di-, and unlithiated bithiazoles (Scheme 3). These compounds are expected to form in a 2:1:1 ratio if the two ends of the dimer react essentially independently. Upon cross-coupling with $\text{Fe}(\text{acac})_3$, the mixture of mono- and dilithiated bithiazoles produces dimer, trimer, tetramer, etc. Gel permeation chromatography (GPC) of the crude product indicated the presence of oligomers from monomer to pentamer (a decathiazole) in the crude mixture; however, only the monomer and dimer (tetrathiazole) were isolated by column chromatography, possibly as a result of the low solubility of the higher propenoxymethyl bithiazole oligomers.

Once isolated, the oligomers are easily identified by NMR. The α -methylene protons of the "monomer" (bithiazole) appear at 4.67 ppm as a singlet; however, the dimer (tetrathiazole) has one set of "inner" CH_2 groups that resonate at 4.59 ppm and two CH_2 groups at the ends of the chain that appear at 4.68 ppm, very close to the value in the monomer. The two different types of α -methylene protons are present in a 1:1 ratio.

Crystallographic Structures. Flat, yellow needles of 4,4',4'',4'''-tetra-(2-propenoxymethyl)-2,2',5',5'',2'',2'''-quater-

- (12) (a) Pappenfus, T. M.; Chesterfield, R. J.; Frisbie, C. D.; Mann, K. R.; Casado, J.; Raff, J. D.; Miller, L. L. *J. Am. Chem. Soc.* **2002**, *124*, 4184. (b) Li, X.-C.; Serringhaus, H.; Garnier, F.; Holmes, A. B.; Moratti, S. C.; Feeder, N.; Clegg, W.; Teat, S. J.; Friend, R. H. *J. Am. Chem. Soc.* **1998**, *120*, 2206.
- (13) (a) Hu, W. P.; Liu, Y. Q.; Xu, Y.; Liu, S. G.; Zhou, S. Q.; Zhu, D. B. *Synth. Met.* **1999**, *104*, 19. (b) Horowitz, G. *Adv. Mater.* **1998**, *10*, 365. (c) Reitzel, N.; Greve, D. R.; Kjaer, K.; Hovs, P. B.; Jayaraman, M.; Savoy, S.; McCullough, R. D.; McDevitt, J. T.; Bjornholm, T. *J. Am. Chem. Soc.* **2000**, *122*, 5788.
- (14) Yamamoto, T.; Maruyama, T.; Zhou, Z.; Ito, T.; Fukuda, T.; Yoneda, Y.; Begum, F.; Ikeda, T. S.; Tahezoe, H.; Fukuda, A.; Kubota, K. *J. Am. Chem. Soc.* **1994**, *116*, 4832.
- (15) (a) Lee, J.; Curtis, M. D.; Kampf, J. W. *Macromolecules* **2000**, *33*, 2136. (b) Gonzalez Ronda, L.; Martin, D. C.; Nanos, J. I.; Politis, J. K.; Curtis, M. D. *Macromolecules* **1999**, *32*, 4558. (c) Nanos, J. I.; Kampf, J. W.; Curtis, M. D.; Gonzalez, L.; Martin, D. C. *Chem. Mater.* **1995**, *7*, 2232. (d) Cao, J.; Kampf, J. W.; Curtis, M. D. *Chem. Mater.* **2003**, *15*, 404. (e) Cao, J.; Curtis, M. D.; Kampf, J. W., manuscript in preparation.
- (16) Koren, A. B.; Curtis, M. D., manuscript in preparation.

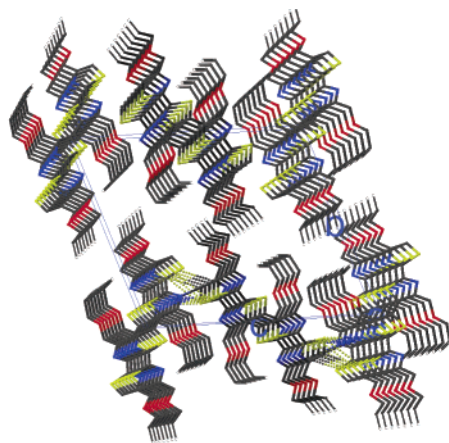


Figure 1. View down the crystallographic a -axis of π -stacked molecules. The molecules are tilted vertically, with respect to the view direction, by $\sim 45^\circ$, as shown in Figure 2.

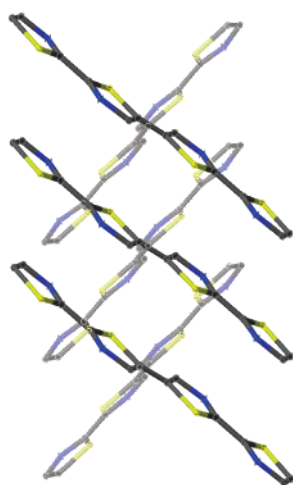


Figure 2. View of π -stacks of **3P2** as projected onto the bc -plane (a -axis is vertical). The darker-shaded molecules are in front of the lighter-shaded molecules.

thiazole (**3P2**) were grown by slow evaporation from an ethanol solution at room temperature. As determined from successful refinement, **3P2** crystallizes in the $P\bar{1}$ space group with two independent molecules per unit cell. Each molecule lies on an inversion center located at $(0, 0, 0)$ and $(0, 0, \frac{1}{2})$. Therefore, the inner rings are strictly coplanar. The outer rings are twisted slightly out of planarity, with respect to the inner rings, by $\sim 3^\circ$; however, the π -orbital overlap between all the rings is very close to its maximum value. The intramolecular bond distances and bond angles are as expected (see Supporting Information). It is the intermolecular contacts and packing motifs that are of interest in the present paper. (Detailed comparisons of the structures of a variety of bithiazole oligomers will be presented elsewhere.^{15e})

When viewed down the crystallographic a -axis, the molecules are π -stacked (interplanar distance of 3.45 \AA) in two, translationally nonequivalent stacks that are canted relative to each other (Figure 1). Figure 2 presents a view perpendicular to the π -stacking axis. The molecules within a given π -stack are tilted ca. 43° , with respect to the stacking axis, causing the molecules to assume a “staircase” structure when viewed at right angles to the molecular plane (Figure 3). Although the molecules are “stepped” relative to one another, the step direction is parallel

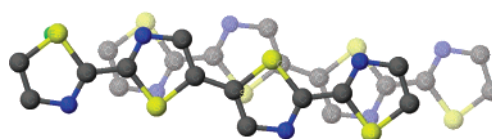


Figure 3. Molecular stacking of **3P2**, as seen perpendicular to the plane of the molecule (side chains removed for clarity). The darker-shaded molecule lies atop the other at a distance of 3.46 \AA .

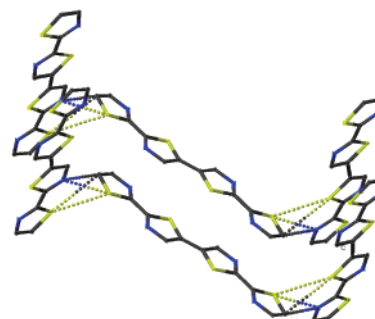


Figure 4. Alternate view of the interstack contacts.

to the long axis of the conjugated ring system, so that there remains appreciable overlap of π -electron density on adjacent rings. This is in contrast to the “herringbone” packing motif, commonly adopted by conjugated molecules, e.g., pentacene and sexithiophene, in which the step direction is along the short axis of the molecule instead of the long axis, resulting in minimal π -overlap.^{9b,17} The closest approaches of a molecule in one stack to a molecule in an adjacent stack are as follows: S–S, 3.71 \AA ; S–C, 3.64 \AA ; S–N, 3.26 \AA ; and N–C, 3.43 \AA (Figure 4). Thus, we might expect a relatively large Davydov splitting in the optical spectra of the solid (see below), because of the relatively strong electronic interactions between the translationally nonequivalent molecules in adjacent stacks.¹⁸

Flat, yellow crystals of 4,4',4'',4'''-tetra-(3-hydroxypropyl-oxymethyl)-2,2',5',5'',2'',2'''-quaterthiazole (**3H2**) were grown by slow evaporation of an ethanol/2-propanol mixture at room temperature. As determined from successful refinement, this compound crystallizes in the $P\bar{1}$ space group with $Z = 1$. Hence, this molecule also lies on an inversion center, located at $(\frac{1}{2}, \frac{1}{2}, \frac{1}{2})$ (Figure 5). As with **3P2**, the inner rings are strictly coplanar and the outer rings are twisted at an angle of 3° from the inner rings; hence, the π -orbital overlap between the rings of a single molecule is close to its maximum value. The molecules of **3H2** also are arranged in slipped π -stacks along the direction of the a -axis (interplanar distance of 3.45 \AA), as in **3P2**. Therefore, alteration of the side chains by oxidation of the propene side group to hydroxypropane changes neither the structure of the conjugated molecular core nor the intermolecular packing of the conjugated rings within a given π -stack (Figure 6). However, the presence of the terminal hydroxy groups on the side chains in **3H2** gives rise to both inter- and intra- π -stack hydrogen bonding. The interstack interactions bind the π -stacks into 2-D sheets parallel to the $(0\bar{1}1)$ planes (Figure 5). Within a given sheet (Figure 7), the hydrogen bonds ($\text{O}\cdots\text{O}$ distances of 2.768 and 2.814 \AA) form an intricate network that binds adjacent molecules vertically in the same stack, in addition

(17) Siegrist, T.; Kloc, C.; Schön, J. H.; Batlogg, B.; Haddon, R. C.; Berg, S.; Thomas, G. A. *Angew. Chem., Int. Ed.* **2001**, *40*, 1732.

(18) Davydov, A. S. *The Theory of Molecular Excitons*; Plenum Press: New York, 1971.

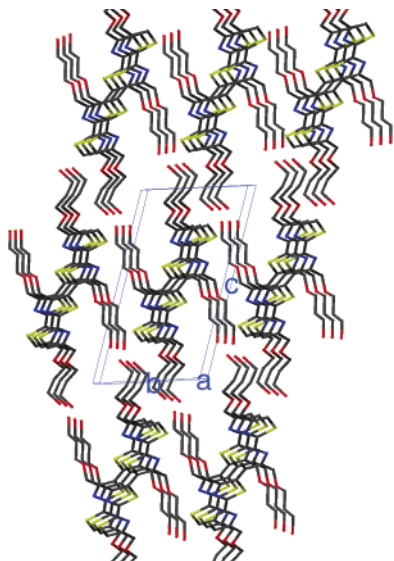


Figure 5. Packing of molecules in **3H2**, as seen down the π -stacking axis (the crystallographic a -axis). Hydrogen bonding links the stacks into 2-D sheets that are parallel to the (011) planes.

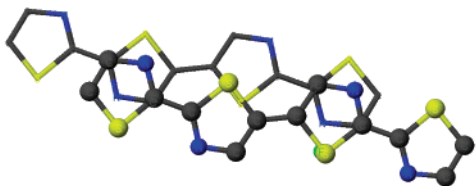


Figure 6. Molecular stacking of **3H2**, as seen perpendicular to the plane of the molecule (side chains removed for clarity).

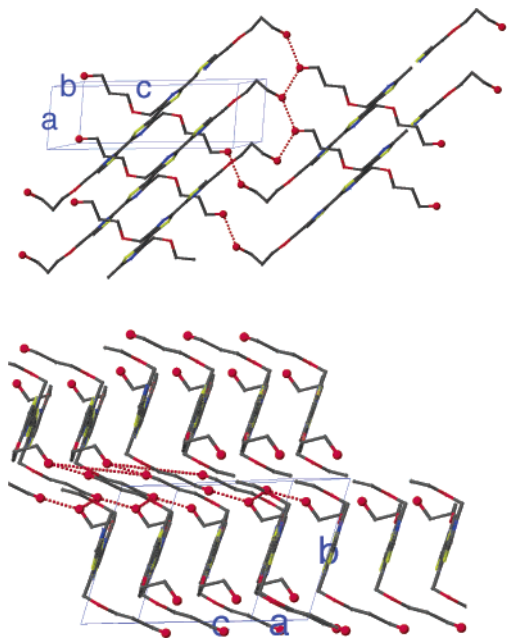


Figure 7. Views down the molecular axes of **3H2** ((top) short molecular axis, approximately perpendicular to the π -stacking axis (crystallographic a -axis); (bottom) long molecular axis, in which the π -stacking direction is along the crystallographic a -axis, which is at an oblique angle in this view).

to connecting molecules in adjacent stacks. The network of hydrogen bonds produces a structure with only one molecule

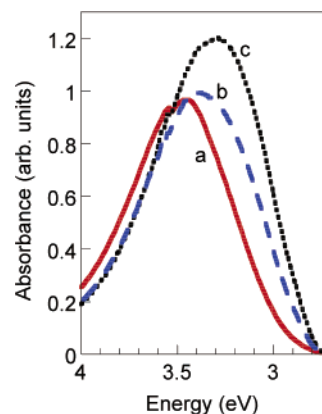


Figure 8. UV-vis absorption spectra of (a) **3P2** in CH_2Cl_2 , (b) **3H2** in CHCl_3 , and (c) **3H2** in CH_2Cl_2 .

per unit cell and minimal electronic interactions between the molecular π -systems in different stacks; i.e., if a π -stack is considered to be a “molecular wire”, the wires in **3H2** are “insulated”, whereas the wires in **3P2** are “shorted”. The fact that all the molecules in the structure of **3H2** are translationally equivalent means that there is no Davydov splitting in the optical spectra of **3H2**.

UV-vis Spectra. The π - π^* transition of most conjugated oligomers and polymers gives rise to a strong absorption in the UV-vis region of the electromagnetic spectrum. In solution and in the solvent-cast film, the two bithiazole “monomers”, **3P** and **3H**, had an absorbance λ_{max} value of ~ 335 nm (3.70 eV), assigned to the ${}^1\text{B}_u \leftarrow {}^1\text{A}_g$ transition. The lack of an appreciable red shift from solution to the solid state indicates that the two thiazole rings are essentially coplanar in solution, so that further planarization is not significant in the solid state. No fine structure was observed in the absorption spectra of **3P** or **3H**, although there was some broadening of the peaks in the film, which may indicate that unresolved transitions are present in the solid-state spectra.

The UV-vis spectra of **3P2** and **3H2** both exhibit strong absorptions ($\epsilon \approx 30\,000 \text{ M}^{-1} \text{ cm}^{-1}$) attributed to allowed π - π^* transitions. As shown in Figure 8, the spectra of **3P2** and **3H2** are not exactly the same in solution. In both chloroform and methylene chloride, **3P2** absorbs at 360 nm (3.44 eV). The λ_{max} value of **3H2**, however, varies with the solvent, appearing at 365 nm (3.40 eV) in methylene chloride and at 375 nm (3.31 eV) in chloroform. Internal hydrogen bonding in **3H2** can explain these variations. The hydroxyl group on the side chain connected to the third ring can hydrogen-bond with either the ether oxygen or the hydroxyl group on the side chain of the first ring. The hydroxyl group pendant off the second ring can likewise hydrogen-bond to the oxygen atoms attached to the fourth ring. These hydrogen bonds create a barrier to the rotation of the rings, keeping the rings more coplanar than in **3P2**. The more coplanar structure leads to the slightly longer wavelength of absorption in **3H2**. The degree of internal hydrogen bonding and, hence, molecular planarity can vary with the polarity of the solvent, thereby influencing the value of λ_{max} .

Figure 9 shows the absorbance spectra of solvent-cast films of **3P2** and **3H2**. For both compounds, there is a shift in the value of λ_{max} from ~ 360 nm (3.44 eV) in dilute solution to longer wavelengths in the solid state, and both spectra exhibit fine structure in addition to being shifted. The spectrum of **3P2**

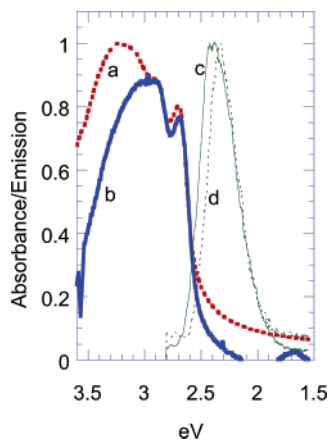


Figure 9. UV-vis absorption and emission spectra of polycrystalline films of **3P2** and **3H2** ((a) absorption spectrum of **3P2**, (b) absorption spectrum of **3H2**, (c) emission spectrum of **3P2**, and (d) emission spectrum of **3H2**).

in the solid film shows a broad absorbance, with peaks at 392, 422, and 459 nm (3.16, 2.94, and 2.70 eV, respectively); however, the spectrum of **3H2** has only the two peaks at 422 and 459 nm.

Many workers have noted that the UV-vis absorption spectra of partially crystalline, conjugated polymers, e.g., regioregular, HT (head-to-tail)-poly(3-alkylthiophenes) (P3ATs), are red-shifted in the solid state, as compared to that in the solution phase, and, concomitantly with the bathochromic shift, the absorption peak (featureless in solution) acquires shoulders or “fine structure”, typically appearing as three “humps” on the absorption peak.^{19,20} In addition to P3ATs, poly(alkylbisoxazoles) (PABOs),²¹ poly(3-octylfuran) (P3OF),²² poly(alkylbithiazoles) (PABTzs),^{15b,c} poly(phenylene-ethynyls) (PPEs),²³ and copolymers containing these chromophores all exhibit the characteristic, three-hump absorption peak profile.^{24,25} There is general consensus that the large red-shift in λ_{\max} is caused by an increase in the effective conjugation length, as a result of the chain backbone becoming more planar in aggregates or the solid state.^{19,20,26,27} However, there is no such consensus on the origin of the fine structure that accompanies the bathochromic shift: the shoulders have been attributed to vibronic coupling²⁸ or to the absorptions of molecules with differing, yet discrete,

conjugation lengths.^{19,20} Recently, solid-state effects (e.g., Davydov splitting and exciton-vibrational coupling) have been recognized as a possible source of the fine structure.^{23b,29,30} A comparison of the spectra of **3H2** and **3P2** gives us a rare opportunity to examine the effects of solid-state packing on otherwise identical $\pi-\pi^*$ chromophores. The hydroxy group in **3H2** is located several carbon atoms removed from the conjugated backbone, so its presence should have very little direct electronic influence on the $\pi-\pi^*$ transition of the rings. The small effect that is observed can be ascribed to internal hydrogen bonding, as described previously. Hence, the markedly different absorbance spectra of the films *must* be related to differences in their solid-state structures and cannot be due to vibronic coupling, differences in conjugation lengths, etc. It is important to note that the absorption spectra of the microcrystalline, solvent-cast films are identical to those of powders made by grinding some of the single crystals from the batch used for the X-ray diffraction study. Therefore, the structural characteristics that lead to multiple peaks cannot be ascribed to a mixture of crystalline and amorphous regions in solvent-cast films.

Molecular exciton theory^{11,31,32} may be used to explain the differences between the absorption spectra of **3P2** and **3H2**. The presence of two molecules per unit cell in **3P2** causes a Davydov splitting (W_D) of all the energy levels into two branches (Figure 10). One component of the Davydov splitting in **3P2** must correspond to the peak at 392 nm, because this absorption is absent in **3H2**. The Davydov splitting can be estimated from the difference between the energies of the two main peaks: $W_D = 3.16 - 2.94 = 0.22$ eV (1810 cm^{-1}). This value is comparable to that found for sexithiophene (T_6), 0.32 eV.³³ The larger value of W_D for T_6 is attributed to the fact that, in T_6 , the interacting transition dipoles lie side by side, whereas they are canted at an angle of $\sim 43^\circ$ in **3P2**. The maximum dipolar interaction occurs when the two dipoles are side by side.

- (19) (a) McCullough, R. D.; Tristram-Nagle, S.; Williams, S. P.; Lowe, R. D.; Jayaraman, M. *J. Am. Chem. Soc.* **1993**, *115*, 4910. (b) Sandstedt, C. A.; Rieke, R. D.; Eckhardt, C. *J. Chem. Mater.* **1995**, *7*, 1057–1059. (c) Chen, T.; Wu, X.; Rieke, R. D. *J. Am. Chem. Soc.* **1995**, *117*, 233–244.
- (20) McCullough, R. D.; Ewbank, P. C. In *Handbook of Conducting Polymers*; Skotheim, T. A., Elsenbaumer, R. L., Reynolds, J. R., Eds.; Marcel Dekker: New York, 1998; pp 243–247.
- (21) Politis, J. K.; Somoza, F. B.; Kampf, J. W.; Curtis, M. D., Gonzalez Ronda, L.; Martin, D. C. *Chem. Mater.* **1999**, *11*, 2274.
- (22) Politis, J. K.; Nemes, J. C.; Curtis, M. D. *J. Am. Chem. Soc.* **2001**, *123*, 2537.
- (23) (a) Bunz, U. H. F.; Enkelmann, V.; Kloppenburg, L.; Jones, D.; Shimizu, K. D.; Claridge, J. B.; zur Loye, H.-C.; Lieser, G. *Chem. Mater.* **1999**, *11*, 1416. (b) Halkyard, C. E.; Rampay, M. E.; Kloppenburg, L.; Studer-Martinez, S. L.; Bunz, U. H. F. *Macromolecules* **1998**, *31*, 8655.
- (24) Politis, J. K.; Curtis, M. D.; Gonzalez Ronda, L.; Martin, D. C.; He, Y.; Kanicki, J. *Chem. Mater.* **1998**, *10*, 1713.
- (25) Huang, W.; Meng, H.; Yu, W.-L.; Pei, J.; Chen, Z.-K.; Lai, Y.-H. *Macromolecules* **1999**, *32*, 118.
- (26) (a) Yang, C.; Orfino, F. P.; Holdcroft, S. *Macromolecules* **1996**, *29*, 6510. (b) Park, K. C.; Levon, K. *Macromolecules* **1997**, *30*, 3175.
- (27) (a) Lambda, J. J. S.; Tour, J. M. *J. Am. Chem. Soc.* **1994**, *116*, 11723–11736. (b) Inganäs, O. *Trends Polym. Sci. (Cambridge, U.K.)* **1994**, *2*, 189–196.
- (28) (a) Sakurai, K.; Tachibana, H.; Shiga, N.; Terakura, C.; Matsumoto, M.; Tokura, Y. *Phys. Rev. B* **1997**, *56*, 9552. (b) Danno, T.; Kuerti, J.; Kuzmany, H. *Front. Polym. Res., [Proc. Int. Conf.]*, **1st** **1991**, 219–222. (c) Yamamoto, T.; Honda, K.; Ooba, N.; Tomaro, S. *Macromolecules* **1998**, *31*, 7.

- (29) (a) Spano, F. C.; Siddiqui, S. *Chem. Phys. Lett.* **1999**, *314*, 481. (b) Spano, F. C. *J. Chem. Phys.* **2001**, *114*, 5376. (c) Spano, F. C. *J. Chem. Phys.* **2002**, *116*, 5877. (d) DiCésare, N.; Belletete, M.; Leclerc, M.; Durocher, G. *Chem. Phys. Lett.* **1998**, *291*, 487. (e) Chen, L. H.; Geiger, C.; Perlstein, J.; Whitten, D. G. *J. Phys. Chem. B* **1999**, *103*, 9161. (f) Langeveld-Voss, B. M. W.; Waterval, R. J. M.; Janssen, R. A. J.; Meijer, E. W. *Macromolecules* **1999**, *32*, 227.
- (30) (a) DiCésare, N.; Belletete, M.; Marrano, C.; Leclerc, M.; Durocher, G. *J. Phys. Chem.* **1999**, *103*, 795. (b) DiCésare, N.; Belletete, M.; Leclerc, M.; Durocher, G. *J. Phys. Chem.* **1999**, *103*, 803. (c) DiCésare, N.; Belletete, M.; Garcia, E. R.; Leclerc, M.; Durocher, G. *J. Phys. Chem.* **1999**, *103*, 3864. (d) Beljonne, D.; Langeveld-Voss, B. M. W.; Shuai, Z.; Janssen, R. A. J.; Meskers, S. C. J.; Meijer, E. W.; Bredas, J. L. *Synth. Met.* **1999**, *102*, 912. (e) Bosio, R.; Botta, C.; Colombo, A.; Destri, S.; Porzio, W.; Grilli, E.; Tubino, R.; Bongiovanni, G.; Mura, A.; DiSilvestro, G. *Synth. Met.* **1997**, *87*, 23. (f) Spooner, S. P.; Whitten, D. G. *Proc. SPIE-Int. Soc. Opt. Eng.*, **1991**, *1436*, 82–91. (g) Penner, T. L. *J. Chim. Phys. Phys.-Chim. Biol.* **1988**, *85* (11–12), 1081–1084.
- (31) (a) McRae, E. G.; Kasha, M. In *Proceedings of the International Symposium on Physical Processes in Radiation Biology* (East Lansing, MI, 1963); Augenstein, L., Mason, R., Rosenberg, B., Eds.; Academic Press: New York, 1964. (b) Giacintov, N. E.; Swenberg, C. E. In *Luminescence Spectroscopy*; Lumb, M. D., Ed.; Academic Press: New York, 1978; p 239ff. (c) Broude, V. L.; Rashba, E. I.; Sheka, E. F. *Spectroscopy of Molecular Excitons*, Springer Series in Chemical Physics, No. 16; Goldanskii, V. I., Ed.; Springer-Verlag: Berlin and New York, 1985. (d) Rebane, K. *K. Impurity Spectra of Solids, Elementary Theory of Vibrational Structure* (in Russ., translated by Scheir, J. S.); Plenum Press: New York, 1970. (e) Kasha, M. *Radiat. Res.* **1963**, *20*, 55.
- (32) (a) Siddiqui, S.; Spano, F. C. *Chem. Phys. Lett.* **1999**, *308*, 99. (b) Manas, E. S.; Spano, F. C. *J. Chem. Phys.* **1998**, *109*, 8087. (c) McRae, E. G.; Kasha, M. *J. Phys. Chem.* **1958**, *28*, 721. (d) Song, Q.; Evans, C. E.; Bohn, P. W. *J. Phys. Chem.* **1993**, *97*, 13736. (e) Evans, C. E.; Song, Q.; Bohn, P. W. *J. Phys. Chem.* **1993**, *97*, 12302–12308. (f) Muccini, M.; Lunedi, E.; Taliani, C.; Beljonne, D.; Cornil, J.; Bredas, J. L. *J. Chem. Phys.* **1998**, *23*, 10513.
- (33) The proper reference state may be obtained with a dilute dispersion of the quaterthiazole in a host lattice of quaterphenyl. See: Blanda, W. M., Ph.D. Thesis, University of Michigan, Ann Arbor, MI, 2000.

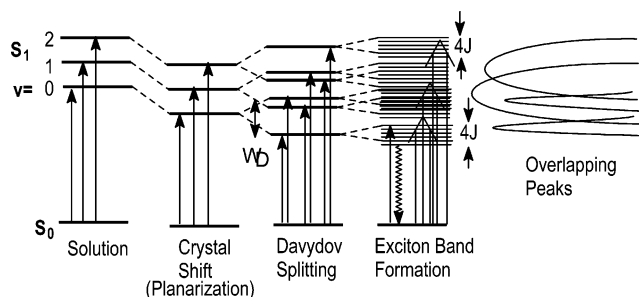


Figure 10. Evolution of the energies of a conjugated molecule, from solution to exciton band formation in a π -stacked solid, and the resulting UV-vis peak profile.

The two peaks at 422 and 459 nm (2.94 and 2.70 eV, respectively) in **3H2** cannot arise from a Davydov splitting, because there is only one molecule per unit cell in **3H2**. The source of these peaks could arise from coupling to vibrational transitions (vibronic coupling), but the peak profiles are not typical of simple vibronic progressions.^{11,22} The more probable source of the multiple peaks is associated with transitions to vibronic states broadened by the exciton band structure that arises from interactions between the translationally equivalent molecules in the π -stacks. The latter interactions spread the energy of each vibronic state into a band with energy (assuming a 1-D stack), $E_k = E_0 + 2J \cos(ka)$, where k is the wave vector ($k = \pi n/Na$, where $n = \pm 0, 1, 2, \dots, N$ and N is the number of molecules in the π -stack), a the intrastack repeat distance, and J the transfer or resonance integral (nearest-neighbor interaction energy, Figure 10). The total width of the band, from $k = 0$ to $k = \pi/a$, is $4J$. For zero-phonon transitions from the ground state to the S_1 excited state, only transitions to the band edge ($k = 0$) are allowed. In J-type “aggregation”, the $k = 0$ state lies at the bottom of the exciton band (J is negative), but in H-type aggregates, the $k = 0$ level is located at the top of the band (J is positive). Hence, compared to an isolated molecule, the absorption of a J-aggregate is red-shifted, whereas that of an H-aggregate is blue-shifted. Experimentally, it is difficult to assess the direction of the shift caused by aggregation when this shift is also convoluted with the red shift caused by planarization of the molecules in the solid state, as in the present case. Our ZINDO/S calculations show that the coupling constant J is positive, so that the absorptions are blue-shifted, relative to an *isolated, planar* molecule; however, the solution spectrum cannot be used as the reference for a planar molecule spectrum, because the molecules are twisted in solution.³³

The basic theory previously outlined predicts one allowed $\Delta k = 0$ transition per molecule in the unit cell. Hence, **3P2** should have two peaks, and **3H2** should have one peak in the spectrum, corresponding to the $\Delta k = 0, \pi - \pi^*$ transition. However, three peaks and two peaks, respectively, are seen in the $\pi - \pi^*$ absorption spectra of **3P2** and **3H2**. The peak shape seen for **3H2**—namely, a low-energy sharp peak superimposed on a broad peak at higher energies—is often seen in the spectra of crystalline materials.^{31d} The narrow peak is assigned to the overlapping set of all $0 \leftarrow 0$ transitions associated with all the coupled vibrational modes. However, the separations between the higher $n \leftarrow 0$ transitions associated with different vibrations are not all the same, the separations being equal to the vibrational frequencies of the coupled vibrations. Hence, these higher $n \leftarrow 0$ peaks are offset by varying amounts. Typically,

only a few vibrational modes are coupled to the $\pi \rightarrow \pi^*$ transition of conjugated oligomers and polymers (these modes being the C=C stretching and ring stretching modes with large amplitude along the molecular axis), so that the first one or two vibronic peaks may be partially resolved.

In the case of π -stacked conjugated molecules, we believe that intermolecular interactions that lead to a breakdown in the $\Delta k = 0$ selection rule further spread out the energies of the vibronic peaks, leading to a completely unresolved, broad peak. As diagramed in Figure 10, each of the $n \leftarrow 0$ vibronic energy levels is spread into an exciton band, because of the intermolecular interactions in the π -stack. Relaxation of the $\Delta k = 0$ selection rule by “two-particle” (electronic plus vibrational) excitations,^{34b} in which the *sum* of the two exciton wave-vectors, $k + k'$, is zero, allows the $n \leftarrow 0$ ($n > 0$) transitions to sample the entire density of states (DOS) of the exciton band. These transitions appear as broad continua centered around the $n \leftarrow 0$ peak positions. If the width of the exciton band, $4J$, is comparable to the separation, $\Delta\nu$, between the vibronic levels, then the continuum states overlap and give rise to a broad, featureless absorption peak, onto which the sharper $0 \leftarrow 0$ peak is superimposed. In **3H2**, we estimate that $4J \approx 0.8$ eV (6450 cm^{-1}) (see below). Therefore, the exciton bandwidth is much larger than any vibrational frequency in the molecule and the vibronic progressions will be completely obscured.^{31a,e}

Line-Shape Model. The line shapes observed in the absorption and emission spectra of crystalline solids are determined by many physical processes. The line shapes are typically significantly broader than those determined by the lifetime of electronic relaxation and often deviate significantly from the Lorentzian line shape expected when relaxation processes alone are the determining factor. Absorption and emission line shapes may be determined by contributions from the electronic DOS, the selection rules governing electronic excitation and relaxation, structural disorder, and the thermal distribution among the initial states.

In the case of molecules arranged in a π -stack, that is, planar π -conjugated molecules arranged with at least a partial cofacial overlap, the molecules of the stack are coupled by a dipole-dipole-type interaction between their molecular transition dipole moments. This coupling is usually referenced as “off-diagonal” coupling, because the coupling matrix elements appear off-diagonal in the matrix representation of the Hamiltonian describing the π -stack. The coupling is often treated theoretically by considering only nearest-neighbor interactions.

Disorder may be introduced into the stack by several processes, including thermally induced lattice motion (phonons), static structural misalignment, or the inclusion of chemical impurities in the aggregate. The disorder will affect both the energy of the individual molecular states (diagonal disorder) as well as the coupling between nearest-neighbor molecules (off-diagonal disorder). Obviously, some types of disorder (structural, chemical defect) are static, whereas others (thermal) are dynamic and temperature dependent. Disorder will affect both the energy states of the stack as well as the probability of excitation from the ground electronic state.

Line shapes for absorption and emission have been computed theoretically by numerical methods and compared with the

(34) (a) Philpott, M. R. *J. Chem. Phys.* **1970**, *54*, 111. (b) Philpott, M. R. *J. Chem. Phys.* **1971**, *55*, 2039.

experimental line shapes. The theoretical line shapes were computed for 1-D π -stacks with cyclic boundary conditions, using experimentally determined parameter values to describe coupling and dynamic (thermal) disorder. The numerical models did not include the effect of off-diagonal disorder or coupling to higher vibrational levels.

A π -stack of N molecules may be described by the following Hamiltonian:

$$H = \sum_i^N |i\rangle \langle \delta_i - E_0 \rangle \langle i| + \sum_{i,j}^N |i\rangle \langle J \rangle \langle j| \quad (1)$$

where $|i\rangle$ designates electronic excitation of the i th molecule in the π -stack, E_0 is the electronic excitation energy of an isolated molecule, and J is the nearest-neighbor dipolar coupling energy. The values of δ_i represent thermal fluctuations of the molecular electronic excitation energy and have a Gaussian distribution with a mean value of zero and a standard deviation of D .

The expression for the absorption intensity of an N -molecule π -stack with Gaussian diagonal disorder is

$$I(\omega) \propto \int \dots \int d\mathbf{e}_1 \dots d\mathbf{e}_N \left[\exp \left(- \frac{e_1^2 + \dots + e_N^2}{2D^2} \right) \sum_{i=1}^N \left(\sum_{j=1}^N A_{ij} \right)^2 \delta(\hbar\omega - E_i) \right] \quad (2)$$

The values of E_i are the eigenvalues of the Hamiltonian and the A_{ij} ($j = 1$ to N) terms are the N components of the i th eigenvector; δ is the Dirac delta function. Equation 2 can be integrated by the Monte Carlo method to obtain a theoretical line shape for various choices of the thermal disorder and the off-diagonal coupling energy.³⁵ Within the framework of this model, it can be shown that the line shape depends only upon the ratio D/J .

Computations were performed by diagonalization of the matrix of the Hamiltonian for π -stacks containing 100 molecules using cyclic boundary conditions. The resulting eigenvalues and eigenvectors were used in the Monte Carlo integration of eq 2. To obtain theoretical line shapes suitable for comparison with experiment, it was necessary to compute Monte Carlo averages over 1000 π -stacks.

In the computation of theoretical emission line shapes, eq 2 was modified to include the thermal distribution of population among the emitting states of the π -stack. For this purpose, it was assumed that thermal equilibrium is achieved among the emitting states prior to electronic relaxation. The aggregate emission line shape is obtained by Monte Carlo integration of the following expression:

$$I(\omega) \propto \int \dots \int d\mathbf{e}_1 \dots d\mathbf{e}_N \left[\exp \left(- \frac{e_1^2 + \dots + e_N^2}{2D^2} \right) \sum_{i=1}^N P_i \left(\sum_{j=1}^N A_{ij} \right)^2 \delta(\hbar\omega - E_i) \right] \quad (3)$$

$$P_i = \frac{\exp[-e_i/(kT)]}{Z(T)} \quad (4)$$

where Z is the partition function for the eigenstates of the π -stack. Monte Carlo integration of eq 3 was performed in a

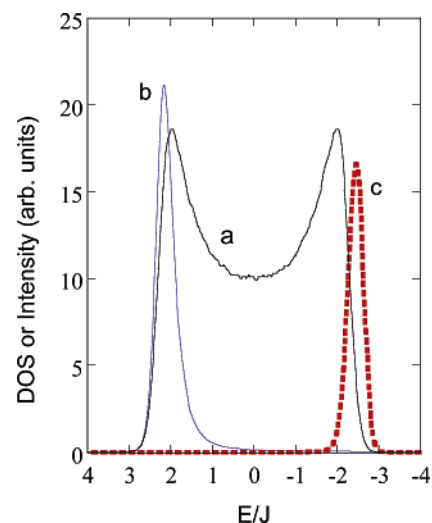


Figure 11. DOS of the $0 \leftarrow 0$ exciton band (plot a), with the calculated absorption (plot b) and (c) emission ($\times 2500$) (plot c) peak profiles superimposed.

manner identical to the integration of eq 2. The results of a typical calculation are presented in Figure 11, in which the calculated line shapes are superimposed on the exciton band DOS.

Comparison with Experiment. The theoretical emission spectrum arises from a Boltzmann distribution of population among the emitting states. Because the model assumes an H-type aggregate, the thermally populated states lie at low energy and are rigorously forbidden in the rigid lattice approximation. Because of the relaxation of the k -selection rules through the participation of thermally excited lattice phonons and low-energy molecular vibrations, the k -selection rules are relaxed and a very weak, long-wavelength emission is predicted. The participation of thermal phonons permits transitions to exciton states of the π -stack that are forbidden in the rigid lattice approximation. The result is a weak absorption into forbidden k -states that extends to the low-energy edge of the exciton manifold. In accord with this model, the observed emission is so weak that we were unable to obtain meaningful measurements of the emission quantum yield. *However, the energy of the experimentally observed emission is found to be significantly higher than that of the theoretically predicted emission.*

The experimental emission peak would lie near the center of the calculated exciton band. This is the energy where we might expect emission from molecules that are not “stacked”, e.g., molecules located at defect sites or at surfaces. Indeed, it has recently been shown that the emission from T_6 films and crystals is dominated by such defect sites.^{32f} If, as the previously mentioned calculations suggest, we assume that the experimentally observed emission peak arises from nonstacked molecules at defect or surface sites and lies near the center of the exciton band, then the energy difference between the high-energy edge of the $0 \leftarrow 0$ peak and the emission maximum is equal to $2J$. Although the high-energy edge of the $0 \leftarrow 0$ peak is not resolved, we estimate that the intercept occurs near 2.8 eV. Thus,

(35) (a) Makhov, D. V.; Egorov, V. V.; Bagatur'yants, A. A.; Alfimov M. V. *Chem. Phys. Lett.* **1995**, *246*, 371. (b) Makhov, D. V.; Egorov, V. V.; Bagatur'yants, A. A.; Alfimov M. V. *Mater. Sci. Eng. C* **1998**, *C5*, 311–315. (c) Schreiber, M.; Toyozawa, Y. *J. Phys. Soc. Jpn.* **1982**, *51*, 1528. (d) Fidler, H.; Terpstra, J.; Wiersma, D. A. *J. Chem. Phys.* **1991**, *94*, 7880.

$2J = 2.8 - 2.33 = 0.47$ eV for **3H2**, and $2J = 2.8 - 2.40 = 0.40$ eV for **3P2**. Thus, values of $J = 0.24$ – 0.20 eV are obtained.

An alternate estimate of the magnitude of J may be made as follows. Assuming that the broad hump at 422 nm (2.94 eV) contains the superposition of the higher vibronic transitions, $n \leftarrow 0$ ($n \geq 1$), each of which is spread into a band of width $4J$, the total width of the absorption peak may be approximated as $W = \mathcal{L} + W_D + 4J$, where \mathcal{L} is the width of the vibronic progression in the absence of broadening by the exciton band and W_D is the Davydov splitting.³⁴ If we assume that the emission comes from defect structures or surface states that are not broadened by the π -stacking (see previous discussion), then the quantity \mathcal{L} may be estimated from the width of the solid-state emission.³⁶ Using this analysis, and with the values $W = 1.3$ eV, $W_D = 0.0$, and $\mathcal{L} = 0.6$ eV for **3H2**, we estimate $4J = 0.7$ eV, or $J = 0.18$ eV (1450 cm^{-1}). The corresponding values for **3P2** are $4J = 1.87 - 0.22 - 0.70 = 0.95$ eV and $J = 0.24$ eV (1930 cm^{-1}); these values are in excellent agreement with those previously obtained.

Previously, vibronic coupling has been used as an explanation of the fine structure seen on the absorption spectra of thiophene and phenylene–vinylene oligomers. As seen in Figure 10, even when intermolecular interactions are important, vibronic coupling does play a role in determining both the breadth and relative intensity of the fine structure on the absorption peak. Furthermore, the relative strengths of vibronic coupling, as measured by the Huang–Rhys factor (γ), versus the intermolecular coupling J and the Davydov splitting W_D , will vary from case to case. If coupling of the electronic transition to an intramolecular vibration is strong, and the intermolecular interactions are weak, then the intensities of the fine structure on the absorption envelope will more closely follow the Poisson distribution ($\gamma^n/n!$) and the peak separations will approximately equal the frequency of the coupled vibrational mode.^{31a} Conversely, strong intermolecular coupling ($J > \gamma$) “washes out” the vibrational contribution and the peak profiles assume the shapes shown in Figure 9. The calculations of Spano et al. predict that the separation between the lowest-energy, $0 \leftarrow 0$ transition and the $1 \leftarrow 0$ vibronic transition increases and may exceed the frequency of the coupled vibration as the intermolecular coupling constant J increases.^{29a,b} In the spectra of conjugated molecules that display the “three-humped” peak profile, the separation between the lowest-energy peak and the central peak is usually larger than the separation between the middle peak and the highest-energy peak. In accordance with Spano’s calculations, the larger separation often exceeds the energies of the highest-frequency ring-stretching modes in the molecule.²² In the case of phenylene–vinylene oligomers, it is possible to fit the fine structure to the superposition of two vibronic progressions.³⁷ It appears that vinylene oligomers and polymers have a $\nu_{\text{C}=\text{C}}$ (vinylene) stretch that has a sufficiently

high frequency ($\nu \approx 1670$ cm^{-1}) to account for the large separation between the two lowest-energy peaks in the absorption spectrum.²¹ Materials that do not contain the vinylene group do not have such high $\text{C}=\text{C}$ (or $\text{C}=\text{N}$) stretching frequencies.³⁸ In the particular case of our bithiazole oligomers, Raman spectra show the absence of any fundamental modes between 1500 and 1800 cm^{-1} (very weak combination/overtone are present at 1600, 1642, and 1700 cm^{-1} in the IR, but these will not couple strongly to the allowed electronic transitions). It is probable that the values of J , W_D , and γ are often comparable in π -stacked structures, so the exact features of the spectral profile will vary case-to-case, according to the dominant interaction(s).^{31e}

The compound 4,4',4'',4'''-tetra-(4-pentenoxyethyl)-2,2',5',-5'',2'',2'''-quaterthiazole (**5P2**) exhibits the same features in its absorption spectra as **3P2**, and 4,4',4'',4'''-tetra-(3-hydroxypropyloxymethyl)-2,2',5',5'',2'',2'''-quaterthiazole (**5H2**) has the same spectrum as **3H2** (see Figs. 1S and 2S in the Supporting Information). The π – π^* chromophore is identical in all these molecules, but each of the side chains of **5P2** and **5H2** have two more carbon atoms than the side chains of **3P2** and **3H2**. The presence of three and two shoulders, respectively, in the spectra of **5P2** and **5H2**, and the pattern of a sharp, low-energy shoulder on the broadened, higher-energy absorptions, suggest that the intermolecular interactions—and, hence, the solid-state packing—in **5P2** and **5H2** are essentially identical to those of **3P2** and **3H2**, respectively.

Thermochromism. The temperature dependence of the absorption spectra is shown in Figs. 3S and 4S in the Supporting Information. As a film of **3P2** is heated past its melting point, the three peaks that are present in the film absorption spectrum at lower temperatures condense into one broad peak at 3.44 eV (360 nm). As this transition occurs, the background absorption is reduced, because the film is more glassy at the higher temperatures and scatters less light, compared to the polycrystalline film. The melted material has an absorption λ_{max} value (360 nm) similar to that found in dilute solution (365 nm). When the hot sample is allowed to cool, the three absorption peaks originally present in the solid reappear. However, the peaks are sharper than those in the original spectrum, suggesting that the thermally annealed film of **3P2** is more crystalline than the solvent-cast film. The oligomer **3H2** is also thermochromic. When the film is almost molten, the fine structure disappears and the absorption λ_{max} value shifts to 365 nm, similar to its value in solution. After the film is allowed to cool, the fine structure reappears, but the peaks are not as sharp as originally observed. Unlike **3P2**, this indicates that the melt-crystallized **3H2** is not as ordered as the solution-crystallized material. The temperature dependence of the absorption spectra of these oligomers is very similar to that of nonylbithiazole oligomers reported previously.^{15c}

Emission Spectra. Unlike the solid-state absorption spectra, the emission spectra of **3P2** and **3H2** (excitation $\lambda_{\text{max}} = 420$ nm) exhibit relatively narrow, almost-featureless peaks at 2.40 eV (517 nm) for **3P2** and 2.33 eV (532 nm) for **3H2** (Figure 12). In addition, **3P2** has a small shoulder at 2.33 eV. The intensities of the emission are very weak and possibly arise from

(36) This approximation assumes that (i) the vibrational frequencies in the S_0 and S_1 states are identical, (ii) each vibronic band is broadened by the same extent, and (iii) all the other sources of line broadening are the same for absorption and emission. The width of the solution absorption spectrum cannot be used to estimate the extent of peak broadening due to all sources other than $4J$, because the solution spectrum is the superposition of the spectra of all the rotamers in solution, whereas only the planar conformation is present in the crystalline solid. See: Curtis, M. D. *Macromolecules* **2001**, *34*, 7905.

(37) Cornil, J.; Beljonne, D.; Shuai, Z.; Hagler, T. W.; Campbell, I.; Bradley, D. D. C.; Brédas, J. L.; Spangler, C. W.; Müllen, K. *Chem. Phys. Lett.* **1995**, *247*, 425.

(38) (a) Hernandez, V.; Losada, S. C.; Casado, J.; Higuchi, H.; Navarrete, J. T. *J. Phys. Chem. A* **2000**, *104*, 661. (b) Louarn, G.; Trznadel, M.; Buisson, J. P.; Laska, J.; Pron, A.; Lapkowski, M.; Lefrant, S. *J. Phys. Chem. A* **1996**, *100*, 12532. (c) Louarn, G.; Trznadel, M.; Zagorska, M.; Lapkowski, M.; Pron, A.; Buisson, J. P.; Lefrant, S. *Synth. Met.* **1997**, *84*, 579.

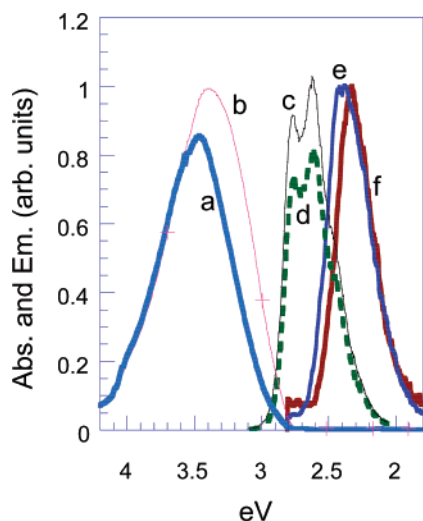


Figure 12. Absorption spectra of (a) **3P2** and (b) **3H2** in dilute methylene chloride, solution emission spectra of (c) **3P2** and (d) **3H2** in dilute methylene chloride, and film emission spectra of (e) **3P2** and (f) **3H2**. The intensities are normalized.

defect sites (see previous discussion). The higher-energy excited states of the S_1 exciton band rapidly relax to the bottom of the band ($k = \pi/a$), and transitions from this state to S_0 are still formally forbidden (Figure 10). The narrow shoulder on the emission peak of **3P2** may be indicative of vibronic structure ($\Delta E = 560 \text{ cm}^{-1}$), in which case the active mode is a bending or librational motion of the backbone. Coupling to these modes in the emission spectra of bithiazole oligomers has been observed previously at low temperature.³³

The excitation maximum of **3P2** (Figure 5S, Supporting Information) is blue-shifted by 18 nm, with respect to its absorption spectrum, and the downward slope of the excitation spectrum is steeper than the slope of the absorption spectrum on the low-energy edge, indicating that transitions at higher energy lead more efficiently to emission. The emission spectra from excitation wavelengths in the range of 380–460 nm (3.26–2.70 eV) all lead to the same emission value, $\lambda_{\text{max}} = 523 \text{ nm}$ (2.37 eV). Thus, transitions to the higher-energy levels relax to the bottom of the exciton band before emission. Similarly, the excitation spectrum of **3H2** is also blue-shifted, relative to its absorption spectrum (Figure 6S, Supporting Information), and excitation from any wavelength in the range of 380–460 nm gives the same emission maximum, at 525 nm.

The solution emission spectra of the dimers are Stokes-shifted, relative to the absorption spectra (1.85 eV for **3P2** and 1.80 eV for **3H2**). This large Stokes shift indicates a large change in geometry between the ground and excited states. The solution emission spectra are blue-shifted, relative to the emission spectra of the films, and the emission from solution is much more intense than that from the film. In dilute solution, the emission maximum occurs at 2.60 eV (477 nm), and a slightly less intense peak at 2.78 eV (446 nm) and a shoulder near 2.47 eV (502 nm) are present for both **3P2** and **3H2**. This shows that the emitting chromophore in solution is the same for both dimers. The energy progression of the fine structure is 1450 and 1290 cm^{-1} . Hence, the source of the multiple peaks may be vibronic coupling to more than one ring stretching mode,³⁹ or the effect predicted by Spano^{29a,b} for the absorption also finds a counterpart in emission. No concentration dependence was noticed for the

emission in the range of 10^{-6} – 10^{-3} M, so aggregate formation is ruled out as a possible cause of the emission fine structure.

Conclusions

Two quaterthiazole oligomers, differing only the nature of their side chains (4,4',4'',4'''-tetra-(2-propenoxymethyl)-2,2',5',5'',2'',2'''-quaterthiazole (**3P2**) and 4,4',4'',4'''-tetra-(3-hydroxypropyloxymethyl)-2,2',5',5'',2'',2'''-quaterthiazole (**3H2**)), were synthesized and shown to crystallize with the molecules arranged in almost-identical π -stacks. The major difference in their solid-state structures, caused by the hydrogen bonding present between the side chains of **3H2**, was that **3H2** had only one molecule per unit cell, as opposed to two in the unit cell of **3P2**. This seemingly minor difference causes a profound change in the appearance of their absorption spectra, which allowed for a rare opportunity to compare directly the absorption spectra of the same chromophore in different but well-defined environments. The observed fine structure results from a combination of Davydov splitting (two molecules per unit cell) and transitions into the density of states of the exciton band structure. The latter is made possible by a relaxing of the $\Delta k = 0$ selection rule by vibronic mixing (two-particle excitation). The pattern of three shoulders is commonly seen in the spectra of crystalline, regioregular polymers, e.g., HT (head-to-tail)-poly(3-alkylthiophenes) (P3ATs) and poly(3-alkylfuran)s. These polymers crystallize in π -stacked structures with two polymer repeat units per unit cell. Such structures would exhibit both Davydov splitting and the spectral features associated with π -stacking. We propose that these typical absorption peak profiles may be regarded as the “optical signature” of π -stacked conjugated structures with two molecules per unit cell.^{40,41} The π -stacked structural motif also leads to enhanced intermolecular transfer (resonance) integrals ($\sim 0.2 \text{ eV}$) that produce wider exciton bandwidths ($4J \approx 0.7$ – 0.8 eV , or 6000 cm^{-1}) than those observed in herringbone-stacked molecules (e.g., pentacene and sexithiophene). If the conduction bands in π -stacked materials are also larger than those of herringbone structures, then π -stacking should produce higher carrier mobilities for organic electronic applications, e.g., thin-film transistors.⁷ Recently, a field effect transistor mobility of $6 \text{ cm}^2 \text{ V}^{-1} \text{ s}^{-1}$ at $25 \text{ }^\circ\text{C}$ was measured in a π -stacked bithiazole oligomer.⁴²

Experimental Section

All reactions were performed under a nitrogen atmosphere, using standard Schlenk-line techniques. Reagents were purchased and used as received unless otherwise stated. ^1H NMR were collected on a Bruker model AM-360, AM-300, or AM-200 spectrometer and referenced to the residual proton solvent resonance. UV–vis spectra were collected on a Shimadzu model 3101PC spectrometer with baseline correction. Films for solid-state spectra were solution-cast onto quartz plates. Emission spectra were collected on a Shimadzu model 4121 spectrometer interfaced with a Gateway computer. Elemental analyses were

(39) Cornil, J.; Beljonne, D.; Heller, C. M.; Campbell, I. H.; Laurich, B. K.; Smith, D. L.; Bradley, D. D. C.; Müllen, K.; Brédas, J. L. *Chem. Phys. Lett.* **1997**, *278*, 139.

(40) (a) Yang, C.; Orfino, F. P.; Holdcroft, S. *Macromolecules* **1996**, *29*, 6510. (b) Park, K. C.; Levon, K. *Macromolecules* **1997**, *30*, 3175. (c) Prosa, T. J.; Winokur, M. J.; McCullough, R. D. *Macromolecules* **1996**, *29*, 3654.

(41) (a) Yamamoto, T.; Lee, B.; Sugauma, H.; Sasaki, S. *Polym. J. (Tokyo)* **1998**, *30*, 853. (b) Aasmundtveit, K. E.; Samuelsen, E. J.; Pettersson, L. A. A.; Inganäs, O.; Johansson, T.; Feidenhans'l, R. *Synth. Met.* **1999**, *101*, 561. (c) Wegner, G. In *Electronic Properties of Polymers*; Kuzmany, H., Mehring, M., Roth, S., Eds.; Springer-Verlag, New York, 185.

(42) Cao, J.; Curtis, M. D., submitted for publication.

performed by the University of Michigan Microanalysis Laboratory. A Scintag model X1 diffractometer, utilizing Cu K α radiation ($\lambda = 0.154$ nm), was used to collect powder and film diffraction data. Films for diffraction were solution-cast onto glass slides.

Synthesis of 4,4'-Chloromethyl-2,2'-bithiazole (1). In a 50-mL, three-neck flask equipped with a stir bar, reflux condenser, and nitrogen adapter, 5.0 g (0.035 mol) of 1,3-dichloroacetone, 2.0 g (0.016 mol) of dithioamide, and 2.0 g (0.024 mol) of calcium carbonate were combined. Under the flow of nitrogen, 20 mL of acetone was added. The mixture was refluxed for 22 h. After this time, the solution fluoresced purple under a "black light" lamp. The flask was cooled, and the product was collected by filtration. The precipitate was washed with cold acetone and then extracted with boiling acetone. The solvent was removed to reveal a brown solid. This solid was sublimed at 125 °C and 0.25 Torr, resulting in a 23% yield of white solid (m.p., 163–164 °C). $^1\text{H NMR}$: $\delta = 7.43$ (s, 1H); 4.73 (s, 2H). MS: $M^+ = 266$, 264. IR (cm^{-1}): 3100, 3016, 2966, 1658, 1553. Anal. Calcd: C, 36.23; H, 2.28; N, 10.56. Found: C, 36.56; H, 2.42; N, 10.53.

Synthesis of 4,4'-Iodomethyl-2,2'-bithiazole (2). In a 100-mL, three-neck flask equipped with a stir bar, reflux condenser, and nitrogen inlet, 20.0 g (0.120 mol) of KI was added to 2.0 g (7.52×10^{-3} mol) of 4,4'-chloromethyl-2,2'-bithiazole suspended in 30 mL of acetone, under the flow of nitrogen. The mixture turned a yellow color. The reaction mixture was refluxed for 3 h. Afterward, the solvent was removed via vacuum. The sample was dissolved in boiling, dry chloroform and then filtered through a 3-cm plug of Celite. The product was then recrystallized, from chloroform at 0 °C, to yield a yellow solid. The product does not fluoresce in solution or after thin-layer chromatography (TLC). Yield: 74%. $^1\text{H NMR}$: $\delta = 7.36$ (s, 1H); 4.55 (s, 2H). MS: $M^+ = 448$. Anal. Calcd: C, 21.64; H, 1.35; N, 6.31. Found: C, 21.85; H, 1.41; N, 5.98.

Synthesis of 4,4'-(2-Propenoxy)methyl-2,2'-bithiazole (3). The lithium salt of allyl alcohol was formed by the addition of butyllithium (2.1 mL of 2.5 M [5.35 mmol] in hexanes) to dry allyl alcohol (0.465 g, 8 mmol) dissolved in 10 mL of tetrahydrofuran (THF) at -78 °C in a 50-mL, three-neck flask equipped with a stir bar, reflux condenser, and nitrogen inlet. The mixture was stirred at -78 °C for 0.5 h. A quantity of 4,4'-iodomethyl-2,2'-bithiazole (0.60 g, 1.34 mmol), dissolved in 25 mL of THF, was then added to the mixture via cannula. The solution was allowed to warm to room temperature, at which point a precipitate formed, and the solution fluoresced blue-purple under a "black light" lamp. The mixture was then refluxed for 2 h. The solvent was removed via vacuum. The product was purified by placing it on a silica gel column and then rinsing it with chloroform. The desired compound was then washed off the column with ether. The light-yellow solid was obtained in an 89% yield (m.p., 53 °C). $^1\text{H NMR}$: $\delta = 7.33$ (s, 1H), 5.96 (m, 1H); 5.33 (d, 1H); 5.23 (d, 1H); 4.68 (s, 1H); 4.13 (d, 2H). $^{13}\text{C NMR}$: $\delta = 161.3$, 155.3, 134.3, 117.55, 117.51, 71.8, 67.9. MS (EI): $M^+ = 308$, 252, 194. Anal. Calcd: C, 54.51; H, 5.23; N, 9.08. Found: C, 54.72; H, 5.48; N, 8.91.

Synthesis of 4,4'-(3-Hydroxypropyloxymethyl)-2,2'-bithiazole (4). In a 100-mL Schlenk flask, 10 mL (5 mmol) of a 0.5 M solution of 9-BBN (9-borabicyclo[3.3.1]nonane) in THF was added via syringe to 0.80 g (2.5 mmol) of 4,4'-(2-propenoxy)methyl-2,2'-bithiazole dissolved in 20 mL of THF. The mixture was stirred for 4 h at room temperature. A solution containing 0.17 g (4.2 mmol) sodium hydroxide and 0.442 g of a 50% solution of hydrogen peroxide (13 mmol) dissolved in 10 mL of water was added slowly via syringe to the flask. The flask became warm. The mixture was stirred for 0.5 h. Another equivalent of the sodium hydroxide/hydrogen peroxide solution was added. More of this solution was added until the flask no longer warmed when additional reagent was added. Ether (50 mL) was added to the flask. The organic and aqueous layers were separated, and the organic layer was then washed twice with 25 mL of water, dried over magnesium sulfate, and filtered. The solvent was removed, and the white precipitate was then washed twice with 100 mL of boiling hexanes. The precipitate

was dried and then dissolved in 5 mL of THF. The solution was added dropwise into 70 mL of hexanes to form a precipitate. The solution was filtered, and the precipitate was dried under vacuum. Yield: 75% (m.p., 103–104 °C). $^1\text{H NMR}$: $\delta = 7.31$ (s, 1H); 4.69 (s, 2H); 3.81 (t, 2H); 3.78 (t, 2H); 2.37 (s, broad, 1H); 1.91 (tt, 2H). $M^+ = 344$. Anal. Calcd: C, 48.76; H, 5.85; N, 7.79. Found: C, 48.02; H, 5.93; N, 8.12.

Synthesis of 4,4',4'',4'''-Tetra-(2-propenoxy)methyl-2,2',5',5'',2'',2'''-quaterthiazole (3P2) (Dimer of 4,4'-(2-Propenoxy)methyl-2,2'-bithiazole). A quantity of 4,4'-(2-propenoxy)methyl-2,2'-bithiazole (0.148 g, 0.48 mmol), dissolved in 15 mL of dry THF, was slowly added via cannula to 0.20 mL of 2.5 M *n*-butyllithium in hexanes (0.50 mmol) dissolved in 5 mL of THF in a Schlenk tube at -78 °C. The mixture turned a deep-purple color as it was stirred for 3 h at -78 °C. Fe(acac) $_3$ was then added in 15 mL of THF via cannula, and the reaction mixture was stirred for 20 min at -78 °C. The mixture was then stirred at room temperature. The solvent was removed under vacuum. The product was purified on a silica gel column using a 70/30 hexanes/ether mixture as an eluent. Yield: 51% (m.p., 81 °C). $^1\text{H NMR}$: $\delta = 7.40$ (s, 1H); 5.92 (m, 2H); 5.26 (m, 4H); 4.70 (s, 2H); 4.59 (s, 2H); 4.15 (d, 2H); 4.08 (d, 2H). MS: $M^+ = 614$. Anal. Calcd: C, 54.69; H, 4.92; N, 8.74. Found: C, 54.49; H, 5.27; N, 9.11.

Synthesis of 4,4',4'',4'''-Tetra-(3-hydroxypropyloxymethyl)-2,2',5',5'',2'',2'''-quaterthiazole (3H2) (Dimer of 4,4'-(3-Hydroxypropyloxymethyl)-2,2'-bithiazole). A quantity of 9-BBN (4.0 mL of 0.5 M in THF, 2.04 mmol) was added via syringe to 3P2 (0.250 g, 0.407 mmol) dissolved in 30 mL of THF in a 100-mL Schlenk flask equipped with a stir bar. The solution was stirred for 7 h. A solution of hydrogen peroxide (1.5 g of a 50% solution) and sodium hydroxide (0.25 g) was degassed and then added via cannula. The flask became warm, and cloudiness was apparent. The reaction mixture was stirred for 1 h. The product was washed three times with 30 mL of water and then filtered to reveal a yellow solid, which was then recrystallized from ethanol. Yield: 80% (m.p., 146 °C). $^1\text{H NMR}$: $\delta = 7.83$ (s, 1H); 4.57 (d, 4H); 4.41 (m, 2H); 3.49 (m, 8H); 1.67 (t of t, 4H). MS (EI): $M^+ = 686$. Anal. Calcd: C, 48.96; H, 5.58; N, 8.16. Found: C, 48.89; H, 5.64; N, 8.03.

Synthesis of 4,4'-Bis(4-pentenoxy)methyl-2,2'-bithiazole (5P). In a 250-mL three-neck flask equipped with a nitrogen inlet, 3.40 mL (33 mmol) of 4-pentenol in 10 mL of THF was added to 9.84 mL (24.6 mmol) of 2.5 M *n*-butyllithium in 30 mL of THF at -78 °C. The mixture was stirred at -78 °C for 0.5 h. To the mixture was then added 3.68 g (8.2 mmol) of 4,4'-diiodo-2,2'-bithiazole dissolved in 100 mL of THF via cannula. The mixture was allowed to warm to room temperature. The volume of solution was reduced to 50 mL under vacuum. The mixture was refluxed for 4 h, and then the solvent was removed under vacuum. The compound was purified by silica gel chromatography, using a 70/30 hexanes/ether mixture as the eluent, to yield a yellow oil as the product. Yield: 60%. $^1\text{H NMR}$: $\delta = 7.31$ (s, 1H); 5.83 (m, 1H); 5.05 (s, 1H); 4.98 (t, 1H); 4.67 (s, 2H); 3.60 (t, 2H); 2.16 (m, 2H); 1.75 (m, 2H). MS: $M^+ = 365$. Anal. Calcd: C, 59.30; H, 6.64; N, 7.68. Found: C, 59.12; H, 6.58; N, 7.42.

Synthesis of 4,4'-(5-Hydroxypentyloxymethyl)-2,2'-bithiazole (5H). The procedure for the synthesis of 4,4',4'',4'''-tetra-(3-hydroxypropyloxymethyl)-2,2',5',5'',2'',2'''-quaterthiazole was followed, with the exception that the product did not precipitate from solution. After the reaction, ether (50 mL) was added to the flask and the organic and aqueous layers were separated. The organic layer was then washed twice with 25 mL of water, dried over magnesium sulfate, and filtered. The solvent was removed. The white solid product was recrystallized from acetonitrile. $^1\text{H NMR}$: $\delta = 7.33$ (s, 1H); 4.68 (s, 2H); 3.75 (m, 1H); 3.65 (t, 2H); 3.60 (t, 2H); 1.74 (m, 2H); 1.62 (m, 2H); 1.51 (m, 2H). MS: $M^+ = 401$. Anal. Calcd: C, 53.97; H, 7.05; N, 6.99. Found: C, 53.58; H, 7.11; N, 6.72.

Synthesis of 4,4',4'',4'''-Tetra-(4-pentenoxy)methyl-2,2',5',5'',2'',2'''-quaterthiazole (5P2). In a 100-mL Schlenk flask, at -78 °C, 0.37 mL (0.93 mmol) of 2.5 M *n*-butyllithium in hexanes was added via

syringe to 0.330 g (0.93 mmol) of 4,4'-bis(4-pentenoxyethyl)-2,2'-bithiazole dissolved in 20 mL of hexanes. The mixture was stirred for 2.5 h at $-78\text{ }^{\circ}\text{C}$. $\text{Fe}(\text{acac})_3$ (0.390 g, 1.1 mmol) in 20 mL of THF was then added via cannula. The mixture was stirred at $-78\text{ }^{\circ}\text{C}$ for 0.5 h and then warmed to room temperature and stirred overnight. The oligomers were separated on a silica gel column using a 70/30 hexanes/ether mixture as the eluent. The dimer (**9**) fraction was produced in 50% yield. $^1\text{H NMR}$: $\delta = 7.39$ (s, 1H); 5.83 (s, 2H); 5.05 (s, 2H); 4.98 (t, 2H); 4.68 (s, 2H); 4.59 (s, 2H); 3.61 (t, 2H); 3.55 (t, 2H). MS: $M^+ = 728$. Anal. Calcd: C, 59.47; H, 6.30; N, 8.02. Found: C, 59.89; H, 6.48; N, 8.02. The tetramer (**10**) fraction, produced in 15% yield, was recrystallized from ethanol (m.p., $121\text{ }^{\circ}\text{C}$). $^1\text{H NMR}$: $\delta = 7.39$ (s, 1H); 5.83 (m, 4H); 5.05 (s, 4H); 4.98 (t, 4H); 4.68 (s, 2H); 4.59 (s, 2H); 3.61 (t, 2H); 3.55 (t, 6H); 2.17 (m, 8H); 1.75 (m, 8H).

Synthesis of 4,4',4'',4'''-Tetra-(3-hydroxypentenoxyethyl)-2,2',-5',5'',2'',2'''-quaterthiazole (5H2**)**. The procedure for the synthesis of 4,4'-(3-hydroxypentenoxyethyl)-2,2'-bithiazole was followed, including the workup. The solid product was recrystallized from 2-propanol in 70% yield. $^1\text{H NMR}$: $\delta = 7.38$ (s, 1H); 4.68 (s, 2H); 4.61 (s, 2H);

3.80 (m, 2H); 3.65 (t, 2H); 3.60 (t, 4H); 3.54 (t, 2H); 1.74 (m, 4H); 1.64 (m, 4H); 1.51 (m, 4H). MS: $M^+ = 800$. Anal. Calcd: C, 54.05; H, 6.80; N, 7.00. Found: C, 53.66; H, 7.12; N, 6.80.

Acknowledgment. This research was supported by the National Science Foundation (DMR No. 9986123). A.K. thanks the NSF for an IGERT Fellowship, provided under DGE Grant No. 9972776.

Supporting Information Available: Crystallographic data for **3P2** (CIF). Structures of **3P2**, **3H2**, **5P2**, and **5H2**. ORTEP drawings of the independent molecules of **3P2** and **3H2**. Tables listing bond lengths and bond angles in **3P2** and **3H2**. Absorption spectra of **3P2**, **5P2**, **3H2**, and **5H2** in films solution-cast from CHCl_3 . UV-vis spectra during heating and cooling of **3P2** and **3H2** films. Excitation and absorption spectra for **3P2** and **3H2** films (PDF).

JA029216M